

Origin of training effect of exchange bias in Co/CoO due to irreversible thermoremanent magnetization of the magnetically diluted antiferromagnet

S. R. Ali,* M. R. Ghadimi, M. Fecioru-Morariu, B. Beschoten, and G. Güntherodt

II. Institute of Physics, RWTH Aachen University, 52056 Aachen, Germany

(Dated: November 10, 2018)

Abstract

The irreversible thermoremanent magnetization ($m_{\text{TRM}}^{\text{irr}}$) of a sole, magnetically diluted epitaxial antiferromagnetic $\text{Co}_{1-y}\text{O}(100)$ layer is determined by the mean of its thermoremanent magnetizations (m_{TRM}) at positive and negative remanence. During hysteresis-loop field cycling, $m_{\text{TRM}}^{\text{irr}}$ exhibits successive reductions, consistent with the training effect (TE) of the exchange bias measured for the corresponding $\text{Co}_{1-y}\text{O}(100)/\text{Co}(11\bar{2}0)$ bilayer. The TE of exchange bias is shown to have its microscopic origin in the TE of $m_{\text{TRM}}^{\text{irr}}$ of the magnetically diluted AFM.

PACS numbers: 75.70.-i, 75.30.Et, 75.50.Ee, 75.60.Nt

* rizwan@physik.rwth-aachen.de

The phenomenon of exchange bias (EB) originates from the interfacial exchange coupling between an antiferromagnet (AFM) and a ferromagnet (FM).[1–3] This interaction results for the magnetic hysteresis loop of the FM layer in a field offset from the origin by the EB field, B_{EB} . EB has been in the focus of intense research activities because of its potential applications in spintronics devices where it stabilizes a reference FM magnetization in magnetic read heads, sensors and nonvolatile memory devices [4, 5]. It has been shown experimentally that field cooling of an AFM stabilizes pinned uncompensated moments near the AFM/FM interface, which are responsible for the EB effect.[6–11] A domain state develops upon field cooling of the AFM, which carries an irreversible surplus thermoremanent magnetization, m_{TRM}^{irr} . The crucial role of m_{TRM}^{irr} at the AFM/FM interface for the EB effect has been demonstrated both experimentally [8–11] and by Monte Carlo simulations.[12] At the surface and in the bulk of the AFM there may be structural and substitutional defects [13], giving rise to domain wall pinning and thus leading to metastable domain structures whose evolution with field cycling is responsible for the training effect (TE). The latter is a crucial feature associated with the fundamentals and applications of EB due to the reduction in B_{EB} during successive field cycles in hysteresis loops.[1, 3] The TE plays an essential role in the reliable performance of devices based on EB. The microscopic origin of the TE remains under intensive debate (see, e.g., Refs. [1–3, 12, 14–18]) and raises the question about the involvement of, e.g., m_{TRM}^{irr} at the AFM/FM interface. However, the smallness of m_{TRM}^{irr} [19, 20] remains a serious difficulty in answering this question.[21] A simple approach might be to consider a sole AFM layer with a dilution enhanced m_{TRM} , i.e. m_{TRM}^{irr} , such that its role for the TE could unambiguously be investigated by magnetometry.

Here, we utilize nonmagnetic dilution throughout the bulk of an epitaxially grown $\text{Co}_{1-y}\text{O}(100)$ layer ($y \rightarrow 0$) to significantly enhance its m_{TRM} . This in turn also yields an enhanced B_{EB} for the corresponding $\text{Co}_{1-y}\text{O}(100)/\text{Co}(11\bar{2}0)$ bilayer. The m_{TRM}^{irr} of a sole AFM layer is then determined by the difference of its enhanced m_{TRM} at positive and negative remanence. The measured m_{TRM}^{irr} exhibits systematic reductions during successive field cycling. Detailed analysis of the data using Binek’s model [14] shows that the TE of B_{EB} of the AFM/FM bilayer has its origin in the TE of m_{TRM}^{irr} of the sole AFM.

Diluted ($y \neq 0$) and undiluted ($y \rightarrow 0$) sole epitaxial AFM samples with the layer sequence: $\text{MgO}(100)/\text{Co}_{1-y}\text{O}(100)/\text{Au}(5 \text{ nm})$ and epitaxial AFM/FM bilayers with the layer sequence: $\text{MgO}(100)/\text{Co}_{1-y}\text{O}(100)/\text{Co}(11\bar{2}0)/\text{Au}(5 \text{ nm})$ were deposited by molecular beam

epitaxy (MBE) on MgO(100) substrates. The samples were capped by a 5 nm thick Au layer and the thicknesses of CoO and Co are 30 nm and 8 nm, respectively. We have chosen CoO as a model AFM for the present study because it allows us to introduce conveniently nonmagnetic defects at the Co sites by just controlling the partial pressure of oxygen ($p(\text{O}_2)$) during the growth of the CoO layer. The over-oxidation of CoO under high $p(\text{O}_2)$ yields a Co^{2+} -deficient layer, Co_{1-y}O . Thus the (intentionally) diluted sample ($y \neq 0$) contains a CoO layer which was grown at a high $p(\text{O}_2)$ ($= 5 \times 10^{-6}$ mbar). On the other hand, the CoO layer in the (nominally) undiluted ($y \rightarrow 0$) sample was grown at low $p(\text{O}_2)$ ($= 4 \times 10^{-7}$ mbar). These pressures were carefully chosen after a number of tests and were found to yield representative values of m_{TRM} and B_{EB} for the respective diluted and undiluted samples.[13]

The epitaxy of our samples has been established in-situ by reflection high energy electron diffraction (RHEED). The RHEED patterns of an undiluted Co_{1-y}O ($y \rightarrow 0$) layer and a diluted Co_{1-y}O ($y \neq 0$) layer grown on the MgO(100) substrate are presented in the insets (a) and (b) of Fig. 1, respectively. The electron beam was parallel to the [010] direction of the MgO(100) substrate. For all the samples the growth of the CoO directly on the MgO(100) substrate leads to untwinned $\text{Co}_{1-y}\text{O}(100)$ layers in this system.[13] For the diluted Co_{1-y}O layers ($y \neq 0$) (grown at $p(\text{O}_2) = 5 \times 10^{-6}$ mbar), the destructive interference of the fcc lattice is removed due to some empty lattice sites caused by the over-oxidation (dilution). Hence, additional diffraction spots become visible which correspond to a crystalline structure with a lattice constant in the real space about twice as large as that of the undiluted CoO (grown at $p(\text{O}_2) = 4 \times 10^{-7}$ mbar). This structure is identified as the Co_3O_4 phase which is formed in the diluted sample due to overoxidation of Co. For AFM/FM bilayers the Co layer grew in an hcp lattice structure with $(11\bar{2}0)$ -orientation (not shown). Magnetic characterization was performed by superconducting quantum interference device (SQUID) magnetometry after the samples were field cooled (FC) from 340 K through the Néel temperature ($T_{\text{N}} = 291$ K) to 5 K in a field of +7 T oriented parallel to the plane of the CoO film along its easy [010] axis. For AFM-only samples the m_{TRM} was recorded as a function of T during the heating of the sample from 5 K to 340 K in the absence of an external field. For AFM/FM bilayers T was increased in steps (from 5 K to 340 K) and a hysteresis-loop was measured between ± 1 T for each step. The coercive fields of the hysteresis cycles B_{C1} for descending and B_{C2} for ascending field branches were used to determine $B_{\text{EB}} = (B_{C1} + B_{C2})/2$.

Figure 1 shows the T dependence of B_{EB} for both undiluted and diluted AFM/FM bilayer

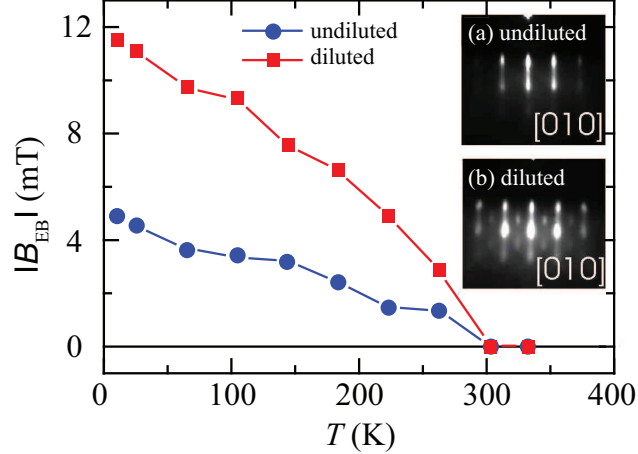


FIG. 1. (color online) Exchange bias field $|B_{EB}|$ of MgO(100)/Co_{1-y}O(100)/Co(11 $\bar{2}$ 0)/Au vs T for undiluted (circles) and diluted (squares) samples. The inset shows RHEED patterns of (a) the undiluted CoO layer and (b) the diluted Co_{1-y}O layer grown on an MgO(100) substrate. The electron beam direction is parallel to [010] of the MgO(100) substrate.

samples. A distinct enhancement of B_{EB} upon dilution is evident below 291 K. However, no change in the blocking temperature, T_B (at which $B_{EB} = 0$), due to dilution was noticed. This is consistent with an up to 5 % dilution of Co²⁺ by Mg²⁺ in Co_{1-x}Mg_xO.[8] The constant T_B we attribute to the high anisotropy of CoO ($\sim 2 \times 10^7$ J/m³, see, e.g., Ref. [22]) which is an Ising-type AFM, making it more robust against magnetic degradation upon dilution. This is in contrast to, e.g., metallic EB systems with low [23] or intermediate anisotropy [9] AFMs which show a more strongly reduced T_B upon dilution.

Figure 2 shows the T dependence of m_{TRM} for both FC diluted (curve I) and FC undiluted (curve II) sole AFM samples. The reference level is set by the zero field cooled (ZFC) diluted sample (curve III). As expected, a strong dilution-induced enhancement ($\sim 400\%$ at 5 K) is observed in the m_{TRM} of the FC diluted sample in comparison to the FC undiluted one. The overall T dependence of the FC m_{TRM} of the diluted sample compared to the undiluted one exhibits two distinct features with decreasing T : (i) a monotonically increasing enhancement between 370 K and 100 K and (ii) an abrupt increase in m_{TRM} for $T < 50$ K. The dilution-induced enhancement of the FC m_{TRM} of sole-CoO layers above 50 K is roughly similar to the one observed for B_{EB} of diluted CoO/Co bilayers in Fig. 1. It is in agreement with the domain state model.[8, 12] However, as opposed to m_{TRM} the entire T dependence of

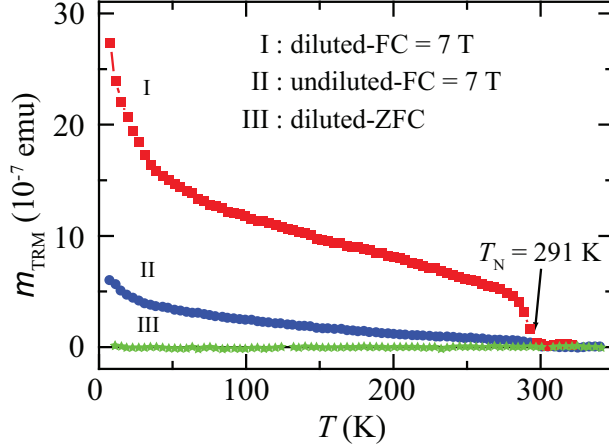


FIG. 2. (color online) Thermoremanent magnetization of field cooled sole-AFM MgO(100)/Co_{1-y}O(100)/Au as a function of T for undiluted (solid circles, II) and diluted (squares, I) samples. The zero field cooled (stars, III) curve of the diluted sample is shown for reference.

B_{EB} is monotonic and it lacks the abrupt increase below 50 K. The difference of $B_{EB}(T)$ and $m_{TRM}(T)$ for $T < 50$ K (Figs. 1 and 2, respectively) is attributed to the low anisotropy of the uncompensated AFM spins [6], which is insufficient to pin the FM layer. This is evidenced by the missing strong increase of the EB field below 50 K (Fig. 1). The "isolated" uncompensated AFM spins freeze in a B field at low temperatures ($T < 50$ K), since they are weakly exchange coupled to neighboring spins within the core of the AFM CoO due to missing or frustrated exchange bonds. The magnetic field stabilizes the uncompensated spins, whereas zero-field cooling does not exhibit any m_{TRM} (see Fig. 1).

We now focus on the cycle number dependence of m_{TRM}^{irr} . A sole diluted Co_{1-y}O(100) sample was cooled from 340 K to 5 K in an external field of +7 T. Subsequently, at 5 K the hysteresis loops were measured by cycling B between -7 T and +7 T. The overall procedure is similar to the measurement of a usual hysteresis loop of an FM. However, during each field cycle, we stop the measurement at $B = 0$ for some time in both the decreasing and increasing field branches. The remanent value of m_{TRM} was then measured (Fig. 3) as a function of time (t) for both ascending (lower curves) and descending (upper curves) field branches. It is evident from Fig. 3 that the m_{TRM} is not constant but that it decreases both as a function of time and cycle number n especially for the descending field branches.

For a given cycle number n the mean of the values of m_{TRM} of the upper and lower curves in Fig. 3 characterizes the vertical shift of the *hysteresis loop* of the AFM layer.[12, 18] The

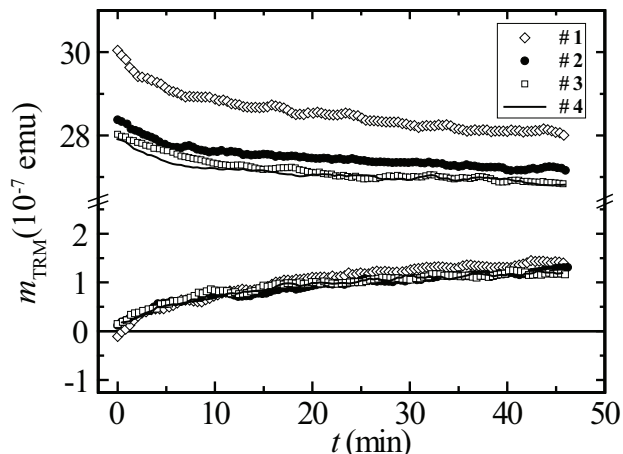


FIG. 3. Thermoremanent magnetization at 5 K of the diluted sole-AFM MgO(100)/Co_{1-y}O(100)/Au sample vs time at $B = 0$ (in remanence) for both ascending (lower curves) and descending (upper curves) field branches of successive hysteresis loop cycles (indicated by #1 - 4). Details about the measurement procedure are described in the text.

vertical shift can be attributed to an additional effective field on the FM, thus yielding EB. We have calculated this mean for $t = 0$, i.e. for the time when the field was set to zero during the AFM hysteresis loop measurement. This quantity measures the irreversible domain state magnetization $m_{\text{TRM}}^{\text{irr}}$ in the whole AFM layer [9, 23] and is plotted as a function of cycle number n in Fig. 4 (open circles). Clearly, the $m_{\text{TRM}}^{\text{irr}}$ is not constant during successive field cycles; instead it decreases monotonically during each cycle.

In order to identify the origin of the EB effect we have also plotted the TE of B_{EB} at 5 K (open squares) in Fig. 4. This was recorded for a diluted Co_{1-y}O(100)/Co bilayer after field cooling at +7 T from 340 K to 5 K. As a reference for our SQUID measurement, we have tested undiluted CoO in a field cooled CoO/Co bilayer at 5 K by exposing it to a reversed field of -0.5 T during waiting times of 0 min. and 60 min. No time dependence of the hysteresis loop was observed. In Fig. 4 a good qualitative agreement is clearly visible between the cycle dependences of B_{EB} and of $m_{\text{TRM}}^{\text{irr}}$ at 5 K. The maximum decrease in both quantities occurs between the first and second field cycle and they asymptotically approach constant values for the remaining cycles. The following empirical formula has been widely used to describe the TE, [24]

$$B_{\text{EB}}(n) - B_{\text{EB}}(\infty) = \frac{k}{\sqrt{n}}, \quad (1)$$

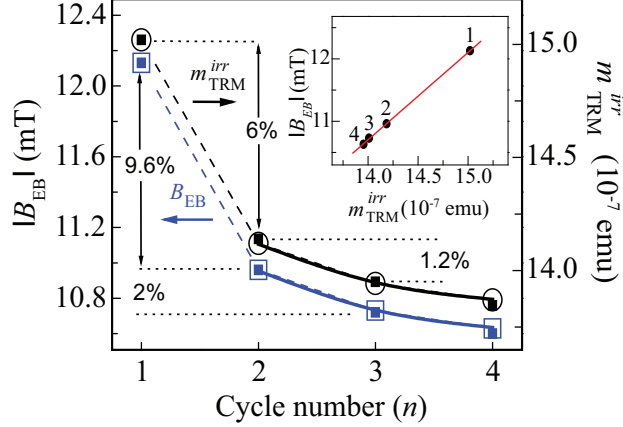


FIG. 4. (color online) Training effect of exchange bias field, $|B_{\text{EB}}|$, of a diluted CoO/Co bilayer (open squares) and of the cycle dependence of $m_{\text{TRM}}^{\text{irr}}$ of a diluted sole CoO layer (open circles) at 5 K. The solid lines show fits by Eq. (1) to the data for $n > 1$. Solid squares are the respective calculated data points generated from Eq. 2. The inset shows $|B_{\text{EB}}|$ vs $m_{\text{TRM}}^{\text{irr}}$ at 5 K; the solid line is a fit to the data points marked by their respective cycle number n .

where k is a material dependent constant and $B_{\text{EB}}(\infty)$ is the EB field in the limit of an infinite number of loops. The solid lines in Fig. 4 show the best fits to B_{EB} and $m_{\text{TRM}}^{\text{irr}}$ data using Eq. 1 for $n > 1$. The resulting parameters obtained from the fit for $B_{\text{EB}}(n)$ are $B_{\text{EB}}(\infty) = 10.2$ mT and $k = 0.8$ mT. Similarly for $m_{\text{TRM}}^{\text{irr}}(n)$ the fitting parameters $m_{\text{TRM}}^{\text{irr}}(\infty)$ and k' were found to be 13.5×10^{-7} emu and 0.6×10^{-7} emu, respectively. The fits clearly show a good agreement with the data for $n > 1$. It should be noted that the experimental data points at $n = 1$ significantly exceed the values obtained by simple extrapolation of the fits to $n = 1$ (not shown). The strong TE of B_{EB} between the first and second hysteresis loop has been attributed to some initial nonequilibrium arrangement or metastable state of the AFM spins.[18, 25–29] The exact mechanism for the initial AFM spin arrangement is still subject to debate. Hoffmann [28] has pointed out that due to biaxial anisotropy axes in the AFM a noncollinear arrangement of the AFM (sublattice) spins can initially be stabilized after field cooling. This leads for perpendicular spin arrangements to a sharp drop in the descending field branch of the first hysteresis loop as the AFM spins relax into a collinear arrangement. Beckmann *et al.* [26] have shown that a misalignment between the cooling field direction and the easy axis of the AFM can result in a nonequilibrium arrangement of the AFM spins with a net $m_{\text{TRM}}^{\text{irr}}$ oriented in a direction determined by the relative orientations

between the cooling field and AFM easy axis. During the field cycling $m_{\text{TRM}}^{\text{irr}}$ tends to find an energetically most favourable orientation via irreversible rearrangements in the AFM spin configuration. This leads to a partial loss of $m_{\text{TRM}}^{\text{irr}}$ and thus of B_{EB} during each cycle, with the maximum decrease taking place during the first cycle.

Although the above dependence of the TE (Eq. 1) has been widely observed, it lacks a physical basis. Alternatively, Binek [14] has considered the TE of AFM/FM bilayers in the thermodynamic framework of spin configurational relaxation at the AFM surface. This spin relaxation is activated by the consecutive cycling of the external field. The following recursive formula is obtained for describing the TE of B_{EB} and $m_{\text{TRM}}^{\text{irr}}$,

$$F(n+1) - F(n) = -\gamma[F(n) - F(\infty)]^3 \quad (2)$$

with F describing B_{EB} (using γ) or $m_{\text{TRM}}^{\text{irr}}$ (using γ'). Taking the respective initial values (for $n = 1$) of B_{EB} and $m_{\text{TRM}}^{\text{irr}}$ as obtained from the experiment (Fig. 4), the calculated data (solid squares in Fig. 4) are obtained from the recursive formula in Eq. 2. For B_{EB} , γ and $B_{\text{EB}}(\infty)$ are 0.05 (mT)^{-2} and 9.26 mT , respectively. Similarly, for $m_{\text{TRM}}^{\text{irr}}$ the parameters γ' and $m_{\text{TRM}}^{\text{irr}}(\infty)$ are $0.08 \text{ (}10^{-7} \text{ emu)}^{-2}$ and $12.8 \text{ (}10^{-7} \text{ emu)}$, respectively. Clearly, Eq. 2 (2) describes the TE of B_{EB} and of $m_{\text{TRM}}^{\text{irr}}$ fairly well, not only for $n > 1$ but also for $n = 1$.

The inset of Fig. 4 shows a direct correlation between $m_{\text{TRM}}^{\text{irr}}$ and B_{EB} for the respective field cycles marked by their number. The solid line represents the best linear fit. The observed correlation between the TE of $m_{\text{TRM}}^{\text{irr}}$ and that of B_{EB} suggests that TE of B_{EB} is due to the loss of $m_{\text{TRM}}^{\text{irr}}$, i.e. due to irreversible changes in the AFM domain state magnetization during the field cycles. It should be noted that during each cycle the percent reductions (see labelings in Fig. 4) in the respective values of $m_{\text{TRM}}^{\text{irr}}$ and B_{EB} do not agree quantitatively. For example during the first field cycle B_{EB} shows 9.6 % reduction in comparison to the 6.0 % reduction of $m_{\text{TRM}}^{\text{irr}}$. These differences are due to some experimental limitations. First, for the case of AFM/FM bilayers the interfacial AFM spins experience in addition to the external field a strong molecular field exerted by the magnetized FM. This results in different strengths of the effective cycling fields on the sole AFM and on the AFM/FM bilayer. Since the molecular fields are typically much stronger ($\sim 100 \text{ T}$) [30] than externally applied fields the AFM spins in the AFM/FM bilayer will experience a stronger effective cycling field. This gives rise to a relatively larger percentage of decrease in B_{EB} of CoO/Co bilayers in comparison to that of $m_{\text{TRM}}^{\text{irr}}$ of the sole CoO sample. Second, our

measured $m_{\text{TRM}}^{\text{irr}}$ includes both volume as well as surface parts of the pinned uncompensated AFM moments, whereas B_{EB} is primarily determined by the pinned AFM moments near the FM/AFM interface. Another factor is the uncertainty in determining the zero of the time scale ($t = 0$) with high accuracy, i.e. when the magnetic field is just switched off and m_{TRM} starts to decay. Significant time (1 - 2 min) was required to reduce the field to zero before the decay of m_{TRM} could be recorded.

In conclusion, our investigation has shown that irreversible thermoremanent magnetization of the sole diluted $\text{Co}_{1-y}\text{O}(100)$ AFM layer exhibits systematic reductions during successive magnetic field cycling which is consistent with the TE of the exchange bias measured for the corresponding $\text{Co}_{1-y}\text{O}(100)/\text{Co}(11\bar{2}0)$ bilayer. Detailed analysis shows that the TE of the exchange bias field of the AFM/FM bilayer has its origin in the TE of $m_{\text{TRM}}^{\text{irr}}$ of the sole AFM layer.

S.R.A. is grateful for funding by the Higher Education Commission (HEC), Government of Pakistan.

-
- [1] J. Nogués and I. K. Schuller, *J. Magn. Magn. Mater.* **192**, 203 (1999).
 - [2] A. E. Berkowitz and K. Takano, *J. Magn. Magn. Mater.* **200**, 552 (1999).
 - [3] J. Nogués *et al.*, *Phys. Rep.* **422**, 65 (2005).
 - [4] B. Dieny *et al.*, *Phys. Rev. B* **43**, 1297 (1991).
 - [5] J. C. S. Kools, *IEEE Trans. Magn.* **32**, 3165 (1996).
 - [6] K. Takano *et al.*, *Phys. Rev. Lett.* **79**, 1130 (1997).
 - [7] P. Miltényi *et al.*, *Phys. Rev. Lett.* **84**, 4224 (2000).
 - [8] J. Keller *et al.*, *Phys. Rev. B* **66**, 014431 (2002).
 - [9] M. Fecioru-Morariu *et al.*, *Phys. Rev. Lett.* **99**, 097206 (2007).
 - [10] L. C. Sampaio *et al.*, *Europhys. Lett.* **63**, 819 (2003).
 - [11] R. Morales *et al.*, *Phys. Rev. Lett.* **102**, 097201 (2009).
 - [12] U. Nowak *et al.*, *Phys. Rev. B* **66**, 014430 (2002).
 - [13] M. R. Ghadimi, B. Beschoten, and G. Güntherodt, *Appl. Phys. Lett.* **87**, 261903 (2005).
 - [14] C. Binek, *Phys. Rev. B* **70**, 014421 (2004).
 - [15] S. Brems, K. Temst, and C. Van Haesendonck, *Phys. Rev. Lett.* **99**, 067201 (2007).

- [16] P. Y. Yang *et al.*, Appl. Phys. Lett. **92**, 243113 (2008).
- [17] A. G. Biternas, U. Nowak, and R. W. Chantrell, Phys. Rev. B **80**, 134419 (2009).
- [18] A. G. Biternas, R. W. Chantrell, and U. Nowak, Phys. Rev. B **82**, 134426 (2010).
- [19] P. Kappenberger *et al.*, Phys. Rev. Lett. **91**, 267202 (2003).
- [20] H. Ohldag *et al.*, Phys. Rev. Lett. **91**, 017203 (2003).
- [21] A. Hochstrat, C. Binek, and W. Kleemann, Phys. Rev. B **66**, 092409 (2002).
- [22] J. Kanamori, Prog. Theor. Phys. **17**, 197 (1957).
- [23] C. Papusoi *et al.*, J. Appl. Phys. **99**, 123902 (2006).
- [24] D. Paccard *et al.*, Phys. Status Solidi **16**, 301 (1966).
- [25] D. Suess *et al.*, Phys. Rev. B **67**, 054419 (2003).
- [26] B. Beckmann, U. Nowak, and K. D. Usadel, Phys. Rev. Lett. **91**, 187201 (2003).
- [27] F. Radu *et al.*, Phys. Rev. B **67**, 134409 (2003).
- [28] A. Hoffmann, Phys. Rev. Lett. **93**, 097203 (2004).
- [29] T. Hauet *et al.*, Phys. Rev. Lett. **96**, 067207 (2006).
- [30] C. Kittel, Introduction to Solid State Physics (Wiley, New York, 1996).